NASA-CR-192136

IN-25-CR
145532
P.10

NASA Research Grant NAGW-1670 Final Report
James P. Reilly, Dept. of Chemistry, Indiana University

I. Free Radical Spectroscopy

In the fall of 1987 during a photoacoustic study of hydrogen peroxide's fourth vibrational overtone band we observed the remarkably clear and well resolved spectrum displayed in Figure 1A. Its periodicity and K subband structure suggested that the spectrum was not of hydrogen peroxide but of a smaller near-prolate symmetric top molecule. Furthermore, the time dependant behavior of the signal indicated that chemical changes were taking place within the photoacoustic apparatus.

A molecule that contains only hydrogen and oxygen and has roughly appropriate rotational constants to match the observed spectrum is the OOH radical. Its ground state rotational constants are as follows:

$A''=20.35656\ cm^{-1}$ $B''=1.117901\ cm^{-1}$ $C''=1.05643\ cm^{-1}$

The radical's large A constant leads one to expect large spacings *between* K subbands. OOH's relatively small and approximately equal B and C rotational constants should lead to small spacings *within* K subbands. Qualitatively, these expectations matched the observed patterns and we tentatively identified the molecule as OOH.

Rotational simulations were then conducted using the literature ground state rotational constants for the OOH radical (Figure 1B). Fine tuning of the upper state rotational constants was accomplished with a simplex least squares optimization program using the assignments and wavelength information from the experimental spectrum. While the overall position of the K subbands was in good agreement with experiment, the line spacings and band head positions within the subbands did not match exactly. A more detailed, high resolution experimental spectrum was necessary before the ambiguity within the K subbands could be resolved.

We recorded high resolution, individual K subband spectra with a Spectra Physics 380D ring dye laser operating single mode with the photoacoustic cell positioned within the laser cavity. A complete spectrum was generated by adding together many smaller overlapping scans each typically 1 cm^{-1} in length. Examples of these high resolution K subband scans are shown in Figures 2 and 3. The dropoff in signal intensity observed for the five R branches at long wavelengths is in part due to chemistry within the photoacoustic cell reducing the population of the radicals. Fewer rotational lines were observed for higher subbands since $J \geq K$. After 5-6 hours all traces of the spectrum disappeared and a hydrogen peroxide spectrum could then be recorded.

Comparison of high resolution experimental spectra and simulations (e.g., Figures 4A and 4B) indicated a serious discrepancy. The spacings within and between P, Q and R branches were clearly not correct. In order to fine tune the upper state rotational constants another simplex least squares optimization was conducted using the more precise high resolution spectral data. Under these conditions the program could not match the data to within its experimental accuracy.

Further manipulation of the simulation's rotational constants provided a clue as to the problem. Much better agreement between experiment and simulation could be obtained by varying *both* the upper and lower state rotational constants. Since this was the case it was no longer clear that OOH was responsible for the

(NASA-CR-192136) FREE RADICAL AND OVERTONE SPECTROSCOPY Final Report (Indiana Univ.) 10 p

N93-21555

Unclas

spectrum that we have been observing.

Our experimental procedure for producing the unknown spectrum was re-evaluated. In order to produce the spectrum it was necessary to completely disassemble, clean and reassemble the photoacoustic apparatus. A photoacoustic cell design that contained o-rings instead of epoxy failed to produce the desired spectrum unless it was first exposed to the epoxy. Mass spectroscopic analysis of the epoxy outgassing products indicated the presence of diethylenetriamine, a primary/secondary amine known to react with peroxides. By introducing pure diethylenetriamine into o-ringed photoacoustic cells that had yielded no data, beautiful spectra were immediately generated.

It was now clear that more elements than just hydrogen and oxygen were present in the photoacoustic apparatus and that the range of possible species capable of producing the rotationally resolved spectrum would have to be expanded. The OOH radical did have a geometry close to what was necessary but increases to both the B and C rotational parameters were found to improve the experimental/simulation agreement. An increase in the B and C rotational constants results from replacing one of the oxygen atoms in OOH with an atom of lower mass. This has the effect of reducing the moment of inertia about the B and C rotational axis and increasing the rotational constants. The A rotational constant is largely unaffected by this change as the mass change is virtually along the A rotational axis.

Of the possible hydrogen, nitrogen, carbon and oxygen arrangements, the molecule HNO became a prime suspect. Rotational constants for HNO have been previously obtained by flash photolysis, microwave spectroscopy, and microwave/visible double resonance methods. These rotational constants are as follows:

$A'=21.95460\ cm^{-1}$	$B'=1.325500\ cm^{-1}$	$C'=1.242600\ cm^{-1}$
$A''=18.46343\ cm^{-1}$	$B''=1.410284\ cm^{-1}$	$C''=1.305649\ cm^{-1}$.

These values were then used to perform another rotational simulation (fig. 4C). The simulation's line spacings were found to be in good agreement with experiment for subbands near the origin. (Other simulated subbands were also in good agreement but they suffer from K-dependant rotational perturbations.)

HNO is known to have an electronic $A^1A''\leftarrow X^1A'$ transition occurring at 760.2 nm. This wavelength compares well with our estimated transition origin of 760 nm. We therefore conclude that we have been recording $A'A''\leftarrow X'A'$ (0,0) spectra of HNO produced by the reaction of H_2O_2 with diethylenetriamine, a component of torr-seal epoxy.

Superb spectra of this transition have already been recorded by Dalby [Can. J. Phys. 36, 1336 (1958)] and Ramsay [Can. J. Phys. 40, 322 (1962)] and we decided that our measurements were not likely to improve the current state of understanding of HNO so this project was terminated.

II. Overtone Spectroscopy

In the last several months we have returned to the vibrational overtone field and have been recording photoacoustic spectra with a new titanium sapphire laser. The $3\nu_1 + \nu_3 + \nu_5$ band of the methyl acetylene is displayed in Figure 5 along with an asymmetric top rotational simulation. Each peak in this spectrum is really an unresolved subband. It is easy to see both the resemblance and the difference between Figures 5A and 5B. The subbands on either wing of this band match the simulation very well while those near the central Q branch appear highly disorganized. Several more subbands are experimentally observed than are

predicted and their intensities are quite irregular. Nevertheless, we were able to assign every peak in Figure 5A. This was accomplished by writing a simple computer program that correlates the lines in the P branch with those in the R branch. By taking advantage of the fact that splittings of rotational energy levels will be manifest in both branches, we were able to construct the energy level diagram displayed in Figure 6 and we assigned quantum numbers to every peak in the observed spectrum. We would like to identify the vibrational state couplings and the exact nature of the vibrational levels that mix in order to produce the observed splittings. While the clear evidence of a J dependence to the splittings might initially suggest a Coriolis coupling mechanism, two facts argue against this. First, the J=0 level of the excited state is split. Second, the P and R branches both *simplify* as the angular momentum quantum number increases. This is opposite of what is expected for Coriolis coupling. Next we considered an anharmonic coupling model. Since the splittings evident in Figure 10A are relative large, (up to about 1 cm^{-1}) we believe that if anharmonic coupling is their source it would probably be a rather efficient (e.g. third or fourth order) process. With a harmonic oscillator basis set, we worked out all possible vibrational levels that could anharmonically couple with $3\nu_1 + \nu_3 + \nu_5$ and that occur within 100 cm^{-1} of its 12764 cm^{-1} position. We found that there were 19 such levels, so at this time we cannot identify which two or three are causing the dramatic effects evident in Figures 5 and 6.

A second intermediate-size molecule that we have been studying very recently is methane. Although the vibrational bands of this spherical top molecule might be expected to exhibit rather simple rotational structure, its $\Delta v=3$ C-H overtone spectrum has only been partially analyzed; all higher overtones are uninterpretable. The source of the observed complexity is not difficult to identify: of the four normal modes of vibration, one is doubly degenerate and two are triply degenerate. As a result, even the fundamental ν_3 and ν_4 infrared bands exhibit complex tetrahedral fine structure due to rotation-vibration interactions. Following considerable theoretical and experimental effort this fine structure is now well understood in the fundamental bands. In fact the ground and first vibrational levels are exceedingly well characterized. However the degeneracies of excited states accessed by overtone transitions are higher. To make matters worse, two of the normal modes are near $1500cm^{-1}$ and two are near $3000cm^{-1}$. The opportunities for anharmonic and Coriolis interactions to split degeneracies and couple various high-lying vibrational states are proliferous.

We have recorded the $3\nu_1 + \nu_3$ overtone spectrum of methane under a few different conditions. The room temperature low resolution (approximately 0.2 cm^{-1}) spectrum is displayed in Figure 7A. In order to reduce the spectral congestion we also recorded this spectrum at 90 K using our cryogenic photoacoustic cell. The result is displayed in Figure 7B. Finally, a simple spherical top simulation, calculated at 90 K, appears in Figure 7C. At the present time we can assign some but not all of the peaks in the experimental spectrum. In the near future we will be extending this work through single mode photoacoustic and molecular beam spectroscopic experiments. A research proposal on this topic has just been submitted to the NASA Planetary Atmospheres division.

Two or three manuscripts will be submitted for publication based on the work described above.

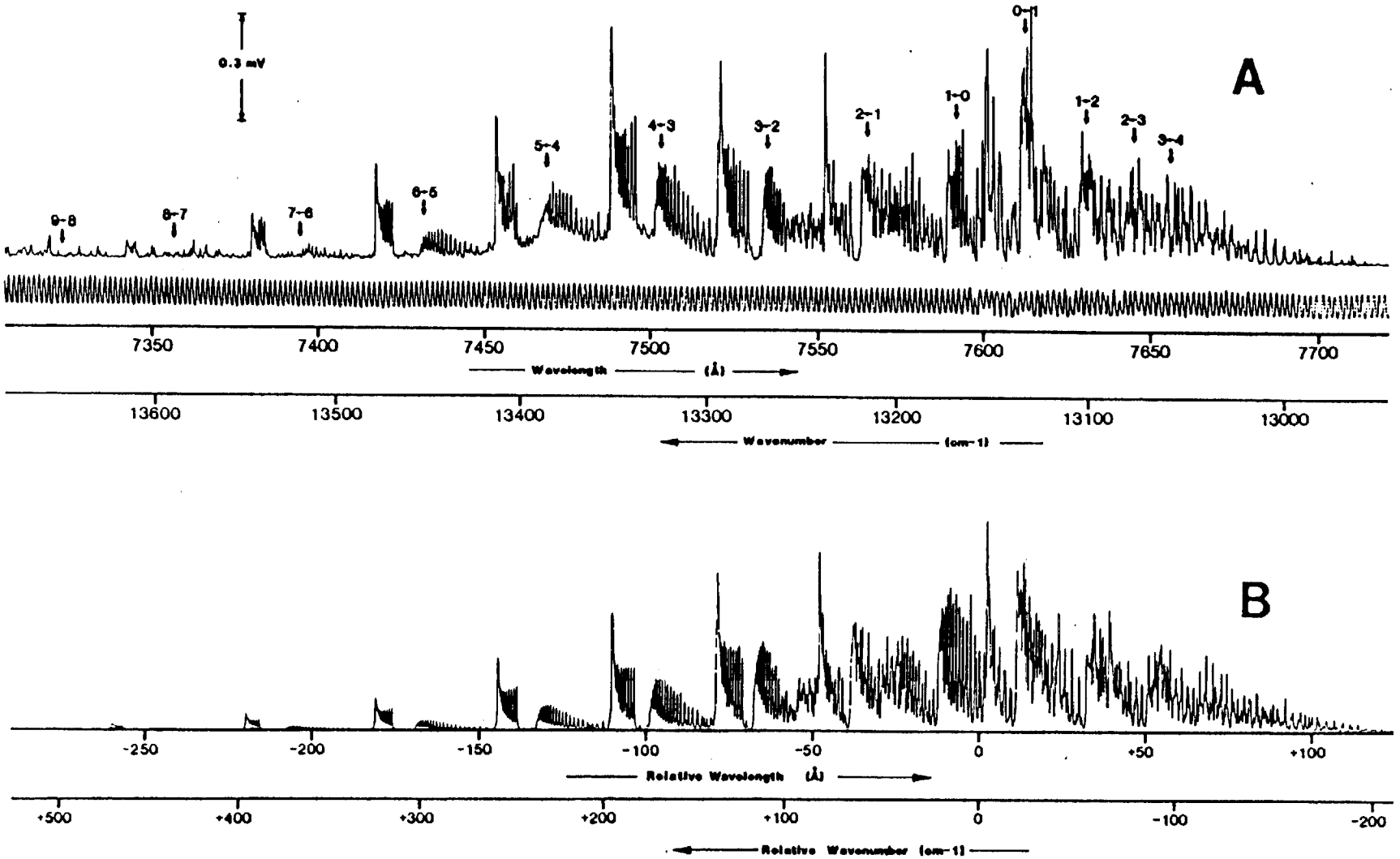

Figure 1: A) Experimental Spectrum B) Simulation

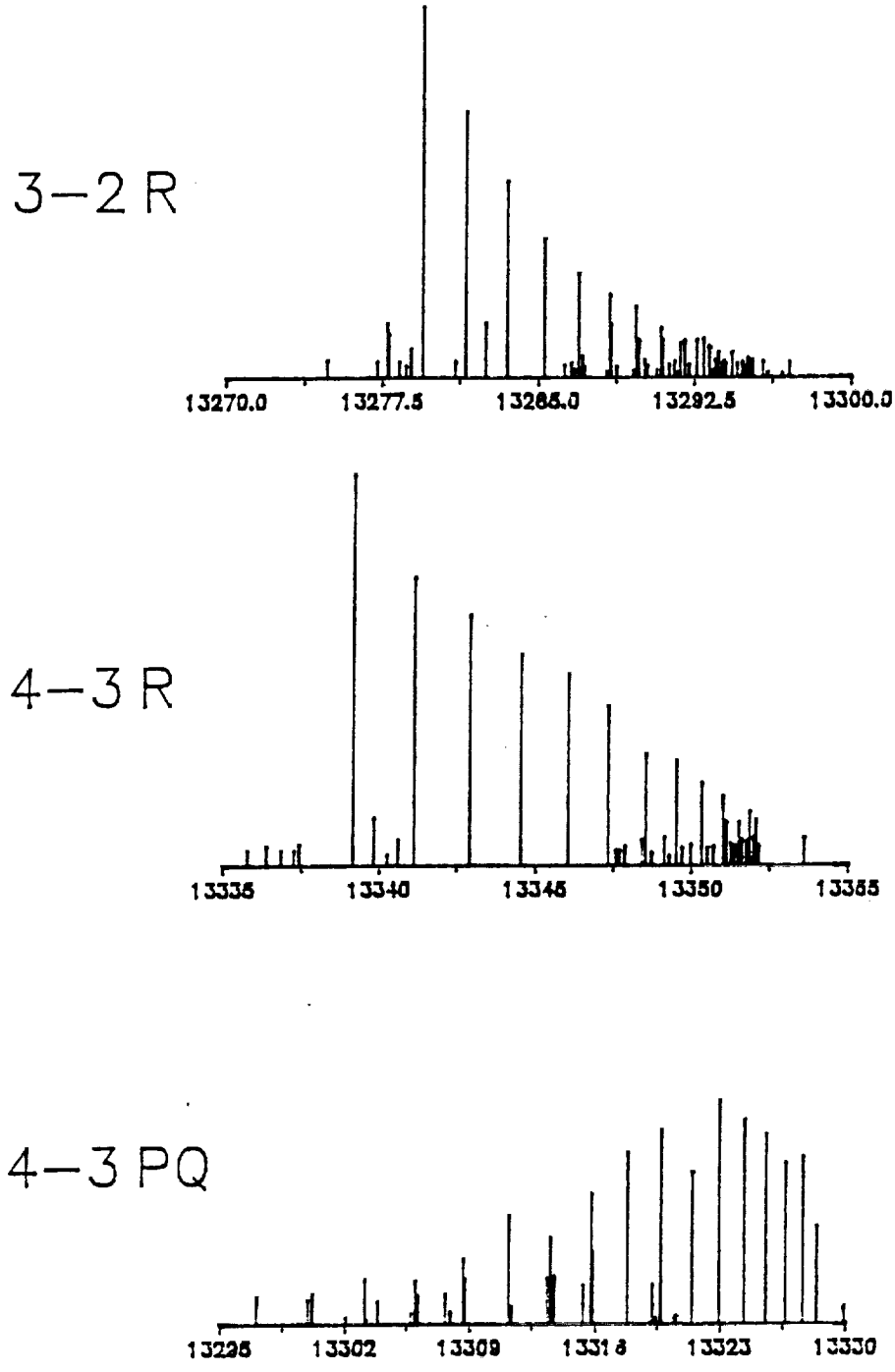

Figure 2: High resolution experimental data (K subbands are labelled)

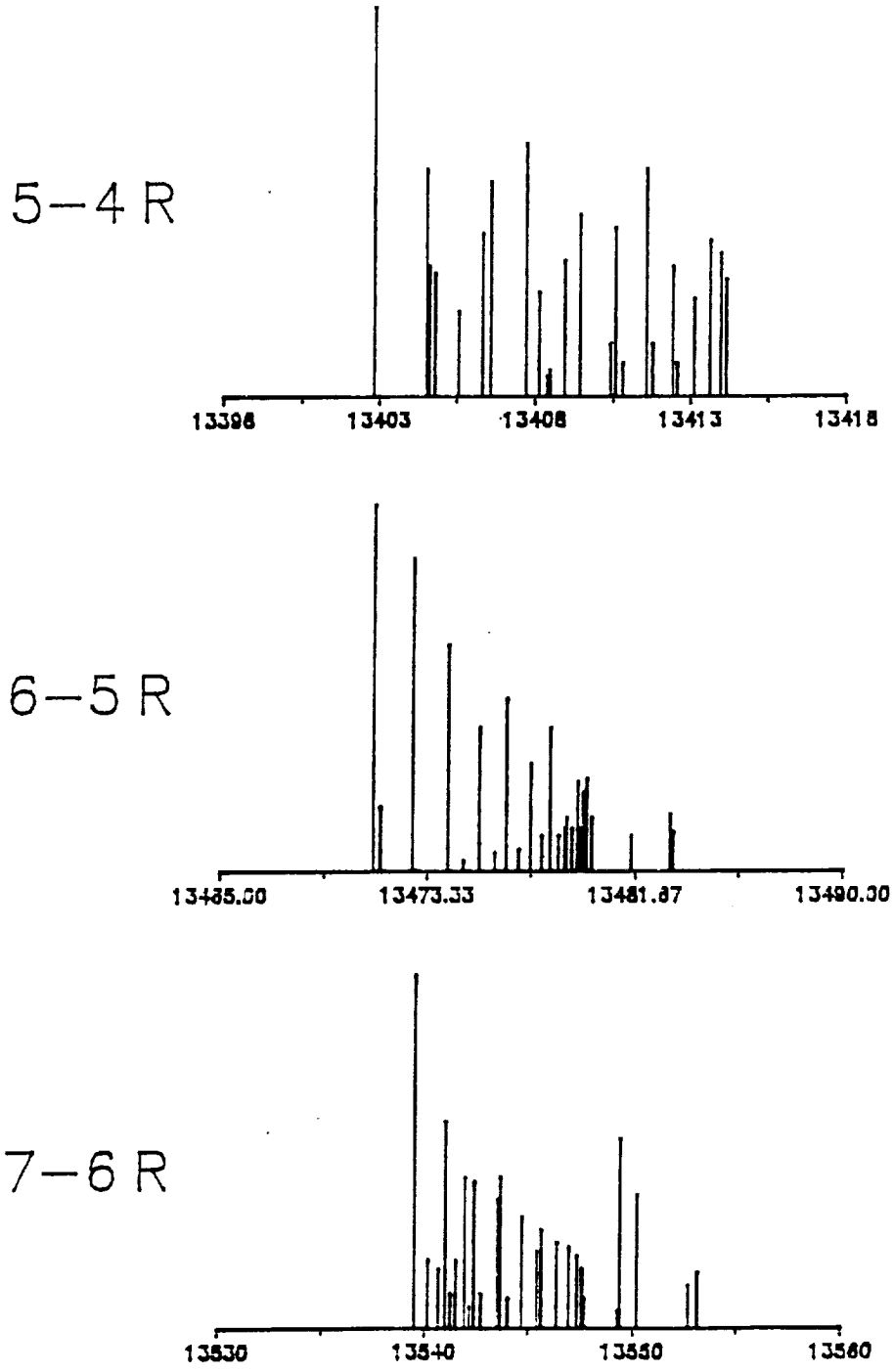

Figure 3: More high resolution experimental data

Figure 4

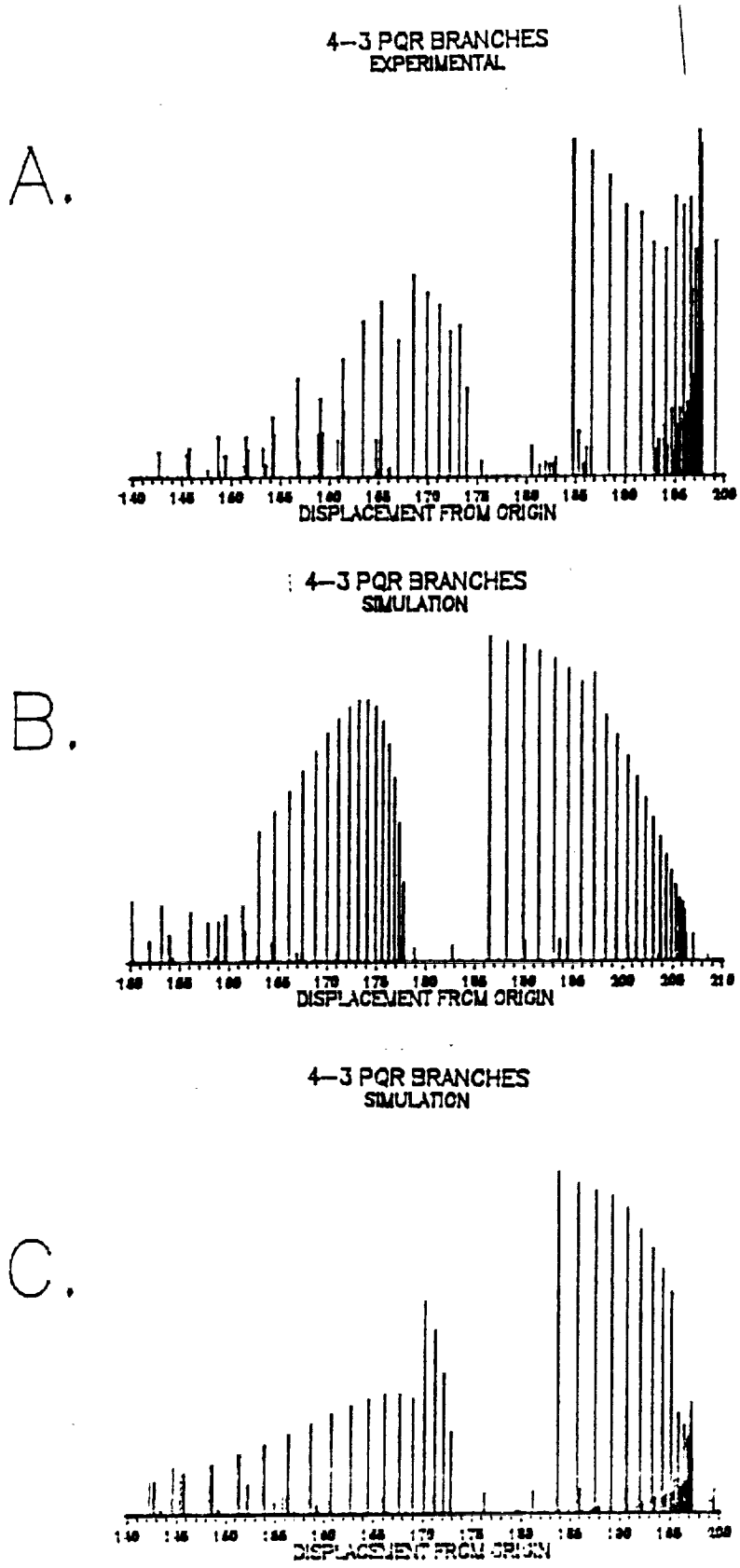
4—3 PQR BRANCHES
EXPERIMENTAL
A.
DISPLACEMENT FROM ORIGIN
4—3 PQR BRANCHES
SIMULATION
B.
DISPLACEMENT FROM ORIGIN
4—3 PQR BRANCHES
SIMULATION
C.
DISPLACEMENT FROM ORIGIN

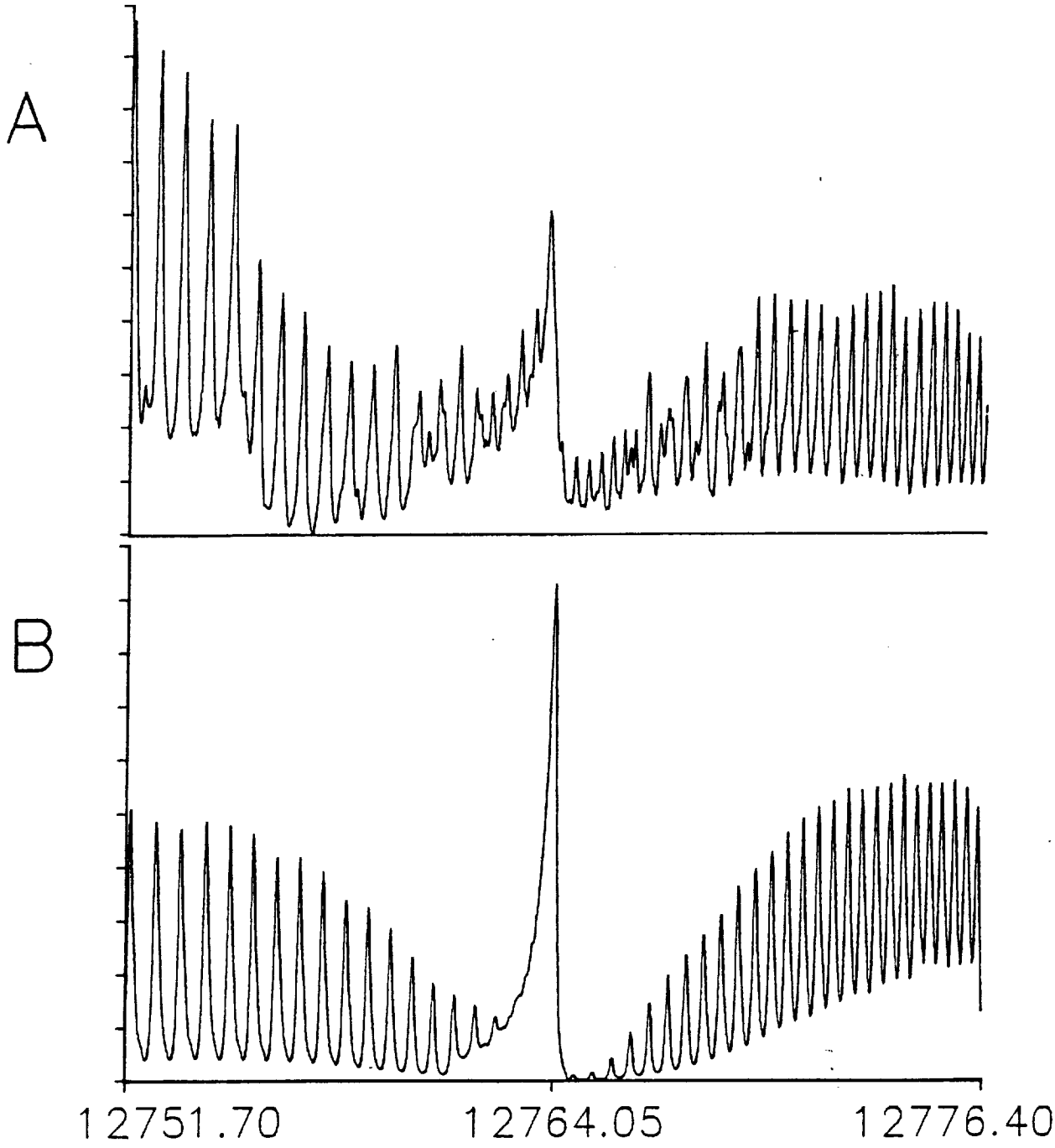

Figure 5: $3\nu_1 + \nu_3 + \nu_5$ vibrational overtone band in the near-infrared. (A) experimental spectrum (B) symmetric top simulation.

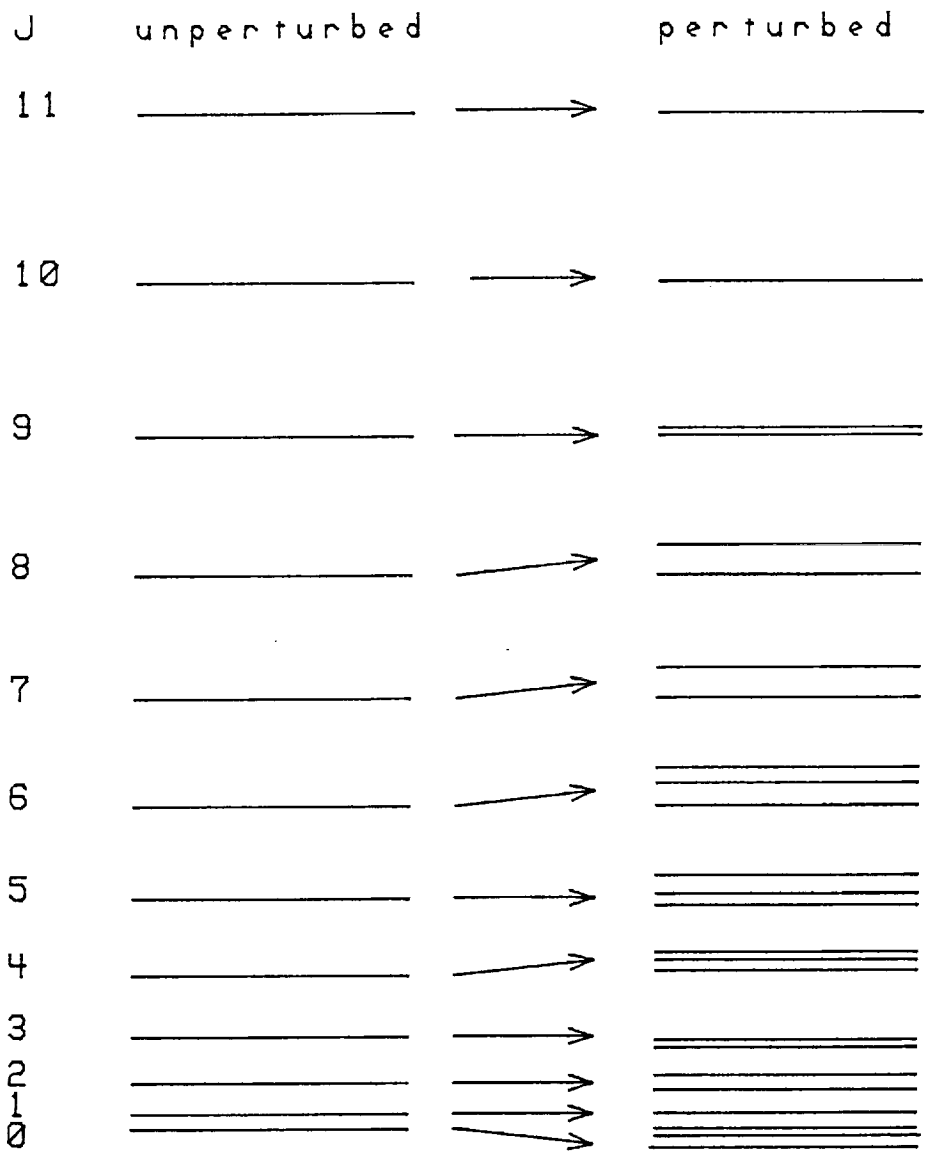

Figure 6: Rotational energy level diagram for the methyl acetylene $3\nu_1 + \nu_3 + \nu_5$ excited vibrational state. On the left are unpeturbed levels predicted by a symmetric top simulation. On the right are the experimentally determined perturbed energy levels, based on an analysis of the spectrum in Figure 10A.

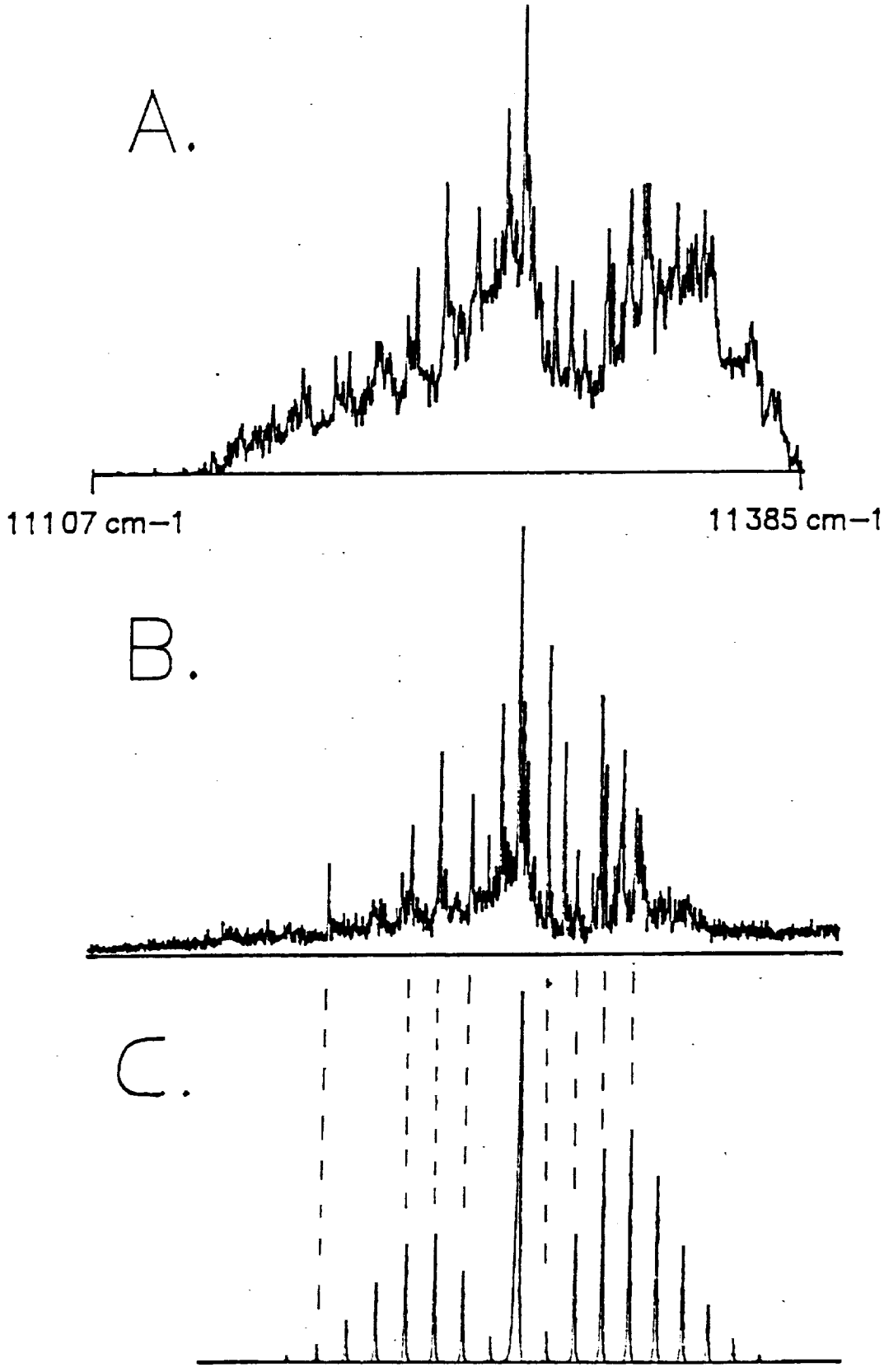

Figure 7 : Bulk gas Δv=4 overtone spectra of methane
(A) 295 K (B) 90 K
(C) 90 K simulation (nuclear spin statistics and tetrahedral fine structure neglected)